Introduction of a "principal stress–weight function" approach to predict the crack nucleation risk under fretting fatigue using FEM modelling

Stéphane Heredia, Siegfried Fouvry, Bruno Berthel, E. Greco

Introduction of a “principal stress - weight function” approach to predict the crack nucleation risk under Fretting Fatigue using FEM Modelling

S. Heredia[1,2)], S. Fouvry[1)*], B. Berthel[1)], E. Greco[2)]

[1)] Laboratoire de Tribologie et Dynamique des Systèmes (LTDS), Ecole Centrale de Lyon, 69134 Ecully cedex, France
[2)] EUROCOPTER, Aéroport Marseille/Provence, 13725 Marignane Cedex, France

[*]Corresponding author: S. Fouvry; Tel.: +33 (0)47218 6562; fax: +33 (0)47833 1140.
E-mail address: Siegfried.Fouvry@ec-lyon.fr

Abstract

The paper discusses a new proposal to predict the crack nucleation threshold under high cycle fretting fatigue using Finite Element Models. This approach displays two main advantages. First, it takes into account the stress gradient induced by the fretting contact. Secondly, the proposed strategy corrects the mesh size dependence of the computed stresses in FEM modelling, so it allows good predictions, and decreases the computation time by increasing the mesh size in the contact area. This original approach is rather simple, combining the study of the maximal stress over a fretting fatigue cycle with a weight function which depends on the stress gradient. The model is tested on quadratic mesh sizes from 5µm up to 100µm, and the results correlate well with experiments. It also shows good capability for predicting crack nucleation conditions for various contact configurations, contact sizes but also various plain fretting and fretting fatigue stresses.

Keywords:

Fretting fatigue, maximal stress, stress gradient, FEM mesh size, Ti-10V-2Fe-3Al

Nomenclature

μ	Coefficient of friction
μ_t	Coefficient of friction at the sliding transition
a	semi contact width
c	semi width of the sticking zone
e	offset of the sticking zone
$k(\ell)$	parameter of the weight function
ℓ	Mesh size
P	Fretting normal load
p_0	Maximal pressure
p_{ref}	Reference maximal pressure
Q	Tangential force
$Q_{(\ell=100\mu m)}$	Predicted crack nucleation threshold with the 100µm mesh size
$Q_{(\ell=5\mu m)}$	Predicted crack nucleation threshold with the 5µm mesh size
Q*	Tangential force amplitude
$Q^*_{CN\_exp}$	Experimental tangential crack nucleation threshold
Q_{CD}	Predicted crack nucleation threshold with the critical distance approach
R	Pad radius
w	weight function
z	depth below the contacting surface
δ	Displacement
δ^*	Displacement amplitude
$\sigma_{1,max}$	Maximal stress over a fretting fatigue cycle
σ_{1,max_c}	Critical maximal stress
σ_d	Alternating bending fatigue limit
σ_{fat}	Applied fatigue stress

1. Introduction

Fretting is associated to a small displacement amplitude between two contacting bodies. Depending on the displacement amplitude, the fretting process is divided into three sliding regimes: the partial slip regime, the gross slip regime and the mixed slip regime [1]. In the case of the large amplitude gross slip condition, wear associated to debris formation and ejection is dominant [2]. Under the partial slip condition, the initiation of fatigue cracks is generally of greater concern than wear [3]. The effect of slip amplitude on the kind of fretting damage can be quantitatively summarized in “fretting map” approaches [4], [5]. Fretting fatigue loading could be characterized by the combination of a heterogeneous cyclic stress gradient related to the contact loading and a homogeneous bulk fatigue loading. From this typical stress distribution cracking processes will evolve in three different ways [6]. Under a threshold fretting fatigue condition, a safe crack nucleation domain is considered where no

cracks are nucleated. Above this threshold two evolutions can be distinguished: for intermediate loading conditions, a crack nucleates; however, due to a very sharp decrease of the contact stress below the interface, it will finally stop. These loading conditions define the safe crack arrest domain [7]. Imposing higher loading conditions leads to a propagation of the nucleated cracks up to total failure. These conditions define the failure domain.

Because of the importance of understanding fretting fatigue, a number of predictive approaches have been developed and applied to formalize crack nucleation boundaries. Approaches are commonly based on multiaxial fatigue models such as the Crossland criterion [8], the Smith-Watson-Topper method [9] and many others. They argue that fretting fatigue loading is always essentially a multiaxial phenomenon, with a contact pressure and surface shearing combined with bulk fatigue stresses. However, local multiaxial fatigue criteria at the surface has failed to compute fatigue strength in the case of sharp stress gradients [10]. This observation led to the use of depth analysis of the stress condition, named “critical distance analysis” [11-14]. Many studies are angled to non-local approaches. Theses approaches are usually based on averaging methods [15-18]. More recently Amargier *et al.* [19] presented a new proposal based on a multiaxial fatigue criterion weighted by a weight function which is directly dependent on the stress gradient under the surface.

This work focuses on the crack nucleation analysis of a Ti-10V-2Fe-3Al titanium alloy subjected to plain fretting and fretting fatigue loading under partial slip condition. First, the crack nucleation threshold is determined, by changing the pad size. Indeed, changing the pad radius leads to a change of the stress gradient below the contact [20]. Fretting fatigue tests were conducted with three different fatigue loadings. Based on experimental results, a finite element analysis was proposed to properly predict the fretting fatigue crack initiation boundary. The first approach detailed in this work is to take into account the stress gradient imposed by the fretting contact by applying a conventional “critical distance” approach. The second one is based on the critical distance methodology adapted with a weight function. The weight function takes into account the stress gradient and is validated for several mesh sizes in FEM. The prediction appears not to be affected by the increase of the mesh size thanks to the introduction of a dedicated weight function which corrects the mesh size effect on the stress computation. Hence, this basic approach allows the stress gradient to be taken into account in the prediction, but it is above all applicable to different mesh size contacts.

2. Experimental procedure

2.1. Material and contact parameters

The chosen material for fretting fatigue samples and pads is a β-titanium alloy named Ti-10V-2Fe-3Al, used in aeronautics for its excellent fatigue properties. The composition of this alloy, in accordance with the ASNA6117 at Eurocopter, is given in *Table 1* and its mechanical properties are shown in *Table 2*.

A plain cylinder on plane geometry has been investigated in this paper with different pad radii, named R1, R2 and R3 where R2 = 2.R1 and R3 = 2.R2. The values of the pad radii are considered as confidential data. A constant width, perpendicular to the sliding direction and high enough to maintain plain strain conditions at the centre (i.e. the median axis) of the fretting scar, is considered. The Hertzian maximum contact pressure varied from about 200MPa to 800MPa but all pressure values are referred to as p_{ref} due to the industrial aspect of this study. In the tested configurations, normal and tangential stresses stayed in the elastic domain of the material. The working frequency is equal to 10 Hz, limited by the actuator's efficiency, but no major effect of the frequency has been observed in past studies [21]. Each test is interrupted at 10^6 cycles because our study is prompted by high cycle fatigue damage.

Table 1
Chemical composition of the Ti-10V-2Fe-3Al (wt. %)

V	Fe	Al	O	N	C	H	Ti
9-11	1.6-2.2	2.6-3.4	< 0.13	< 0.05	< 0.05	< 0.015	Balance

Table 2
Mechanical properties of the Ti-10V-2Fe-3Al

Elastic modulus (GPa)	110
Poisson ratio	0,32
Yield stress (MPa)	1050
Density (g/cm^3)	4,65
Hardness (HB)	320
Alternating bending fatigue limit, σ_d (MPa)	575

2.2. Plain fretting and fretting fatigue set-ups

Figure 1 shows a schematic drawing of the plain fretting test used in this study. A tension-compression hydraulic machine is used to impose the displacement between the plane and the cylindrical pad. Further details of this setup and experimental methods used can be found in [22]. A constant normal force P is applied. The cyclic sinusoidal displacement δ is then applied to generate an alternating tangential load Q on the contact. During these fretting tests, the displacement δ, the normal force P and the tangential force Q are recorded. In the partial slip regime, an increase of the displacement amplitude δ* leads to an increase of the tangential force amplitude Q*. In the gross slip regime, the Q*/P ratio stays constant for any displacement amplitude and is correlated to the friction coefficient μ of the contact.

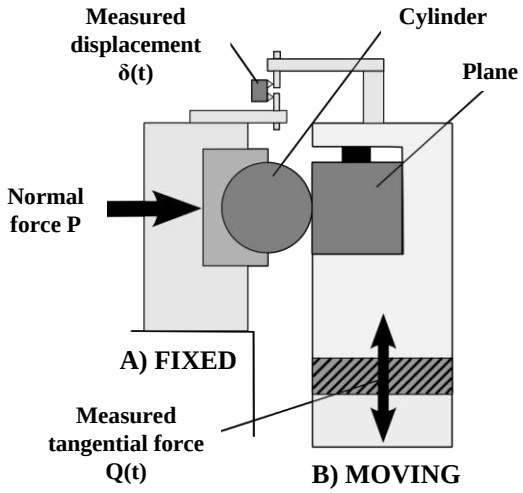

Figure 1. Plain Fretting Test System

The fretting fatigue experimental set-up is represented in Figure 2. It was inspired by the experimental set-up designed by Hills *et al.* [23] and the one developed by Mall *et al.* [24]. It is a dual actuator device that allows the separate application of the fretting condition and the fatigue load. Multiple sensors allow the following parameters to be recorded during tests: the fretting and the fatigue loads (Q and σ_{fat}), the fretting and the fatigue displacements, and the fretting normal load (P). Further details of this setup and the experimental methods used can be found in [25].

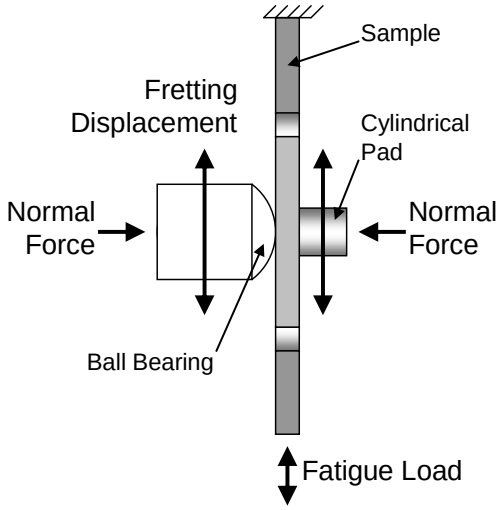

Figure 2. Fretting fatigue dual actuator device

As long as a partial slip condition is imposed (i.e. $Q^* < \mu_t.P$), applying an alternating tangential force promotes a composite interface structure with an inner central sticking zone bordered by lateral sliding zones (Figure 3.a). As demonstrated by Nowell *et al.* [26], under fretting fatigue the bulk loading which is present in the fatigue specimen but not in the pad specimen promotes a mismatch in strains. The result of this couple effect of the fatigue loading on the partial slip fretting contact is the introduction of an offset of the centre of the sticking zone from the centre of the contact. By contrast to the plain fretting condition, the dissymmetry of the sliding distribution promotes a larger sliding domain at the trailing edge of the contact (Figure 3.b). The offset of the sliding zone for a 2D cylinder on plane configuration is given by [7]:

$$e = \frac{\sigma_{fat} \cdot a}{4 \cdot \mu \cdot p_0} \qquad \textbf{(1)}$$

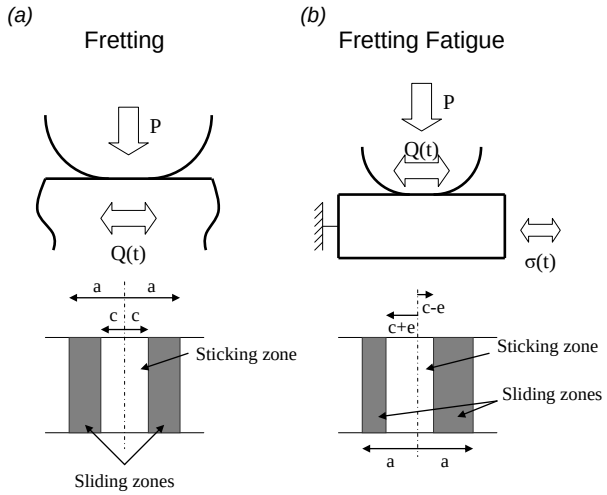

Figure 3. Contact area: (a) plain fretting and (b) fretting fatigue; e: offset of the sticking zone

2.3. Post-test cracking analysis

All of the tests presented in this paper were interrupted at 10^6 cycles and analysed. Analyses consisted in determining of the crack depth through cross section observation. This crack analysis technique has been inspired by Proudhon *et al.* [17]. The sample is cut in the middle of the scar. Then, the newly created surface is polished and observed with an optical microscope. The polishing and observation phase is repeated three times in order to evaluate the homogeneity of the crack length. The polishing process gives spacing between two observation layouts of about 500 µm (Figure 4). For fretting tests, the scale of crack depths studied is from 0 to about 500 µm. Therefore, the technique used is sufficient to obtain proper quantification of the crack depth. For fretting fatigue experiments, the cracks extend much further and the assessments have shown less homogeneous crack dimensions. That is why the observations were taken from ten polishing planes instead of just three.

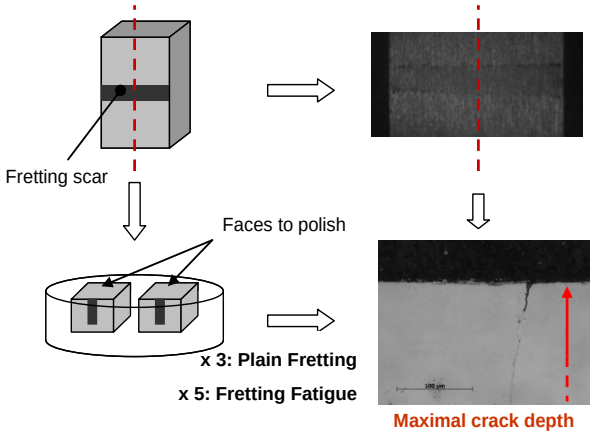

Figure 4. Experimental method to investigate cracking after plain fretting and fretting fatigue tests; see the text for details

2.4. Quantification of the experimental crack nucleation

Whatever the plain fretting or fretting fatigue stressing conditions, cracks nucleate at the edges of the contact where the maximum tensile stresses are imposed. The experimental work of this paper consists in investigating crack nucleation in plain fretting and fretting fatigue loading under partial slip contact. In this set up, contact parameters are fixed and the only varying parameter is the tangential loading. The crack nucleation threshold is determined for a constant cylinder radius and a constant contact pressure (a crack is considered when it is deeper than 5µm).

First used for the plain fretting condition, this methodology was applied for three contact pressures for the smaller pad R1 and only one contact pressure $p_0 = p_{ref}$ for the two others pad radii (R2 and R3). Fretting fatigue tests were performed with the two larger pads (R2 and R3) and a constant maximal pressure fixed at p_{ref}. In this part, three fatigue stress levels were defined. For each fatigue level, different experiments were performed, varying the tangential condition, in the same way as for plain fretting experiments, in order to determine the cracking conditions (Figure 5).

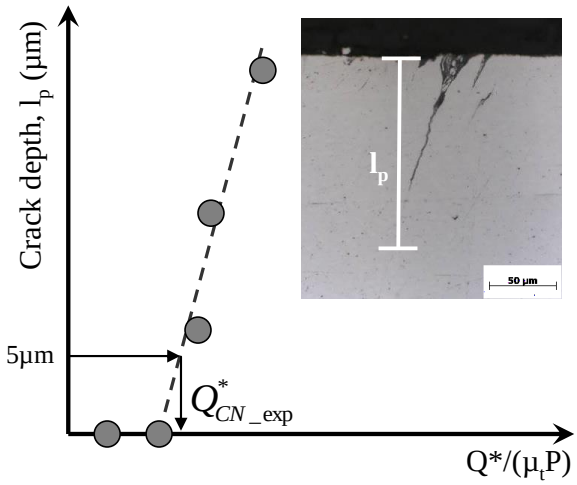

Figure 5. Illustration of the determination of the crack nucleation threshold as a function of the applied tangential force loading: plain fretting ($\sigma_{fat} = 0$); fretting fatigue ($\sigma_{fat} \neq 0$)

For each contact condition, an experimental crack nucleation threshold $Q^*_{CN\_exp}$ is thus defined. Table 3 summarizes the experimental crack nucleation thresholds for plain fretting conditions and

Table 4 summarizes the crack nucleation conditions for fretting fatigue loadings.

Table 3
Fretting crack nucleation thresholds ($\sigma_{fat}/\sigma_d = 0$)

Pad	p_0/p_{ref}	$Q^*_{CN\_exp}/(\mu_t.P)$
R1	1.36	0.70
R1	1.55	0.54
R1	1.75	0.48
R2	1.00	0.94
R3	1.00	0.72

Table 4
Fretting fatigue crack nucleation thresholds ($p_0/p_{ref} = 1.00$)

Pad	σ_{fat}/σ_d	$Q^*_{CN\_exp}/(\mu_t.P)$
R2	0.07	0.75
R2	0.13	0.54
R2	0.27	0.26
R3	0.07	0.53
R3	0.13	0.40
R3	0.27	0.17

3. Crack nucleation prediction in FEM

3.1. Model geometries

Finite element models have been defined using the commercial ABAQUS software. Only a bi-dimensional, elastic, standard analysis is defined in relation to the contact properties. The normal and tangential loads correspond to the experimental ones and are applied on top of the cylindrical pad, taking into account the imposed displacements conditions.

Figure 6 illustrates the FEM model of the plain fretting test, related to the smallest pad R1. The fretting model is composed of a fixed plane and a moving cylindrical pad. The mesh is composed of triangular (CPE3) and quadratic (CPE4R) linear elements. Quadratic elements are used to define the contact zone in a square domain of about 500µm in depth and from -2a to 2a in length. Their size is 100µm long by 100µm deep. Outside the contact zone triangular elements are considered in order to reduce time costs. The contact is described by a master-slave algorithm and the tangential loading is determined by Lagrange multipliers through a constant friction coefficient. This latter variable corresponds to the coefficient of friction at the sliding transition μ_t experimentally determined. During a computation, a fretting cycle is reproduced through the introduction of a normal load P and through the application of a cyclic tangential cycle.

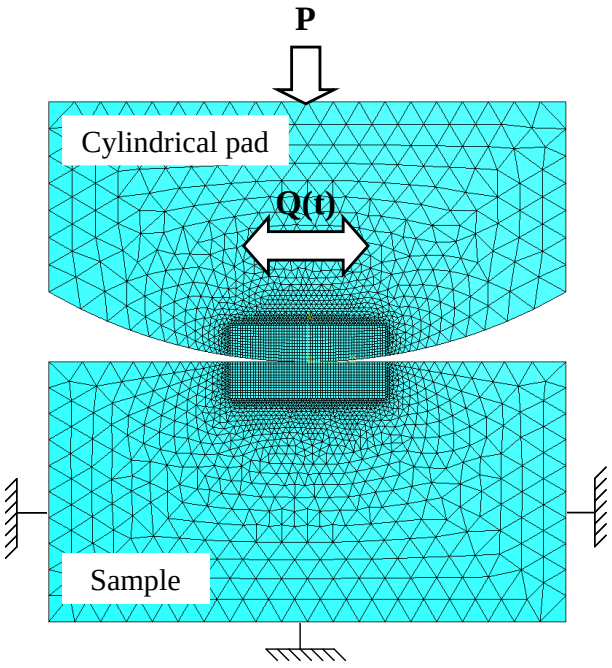

Figure 6. FEM fretting model; radius of the pad: R1; contact mesh size ℓ=100µm

The equivalent ℓ = 100µm of the FEM model related to the fretting fatigue configuration is given in Figure 7. It represents a part of the sample, the ball-bearing and the cylindrical pad. Contact between the ball-bearing and the sample is frictionless whereas a coefficient of friction is introduced into the pad/sample contact. Like for plain fretting configurations, contact areas were meshed using quadratic elements.

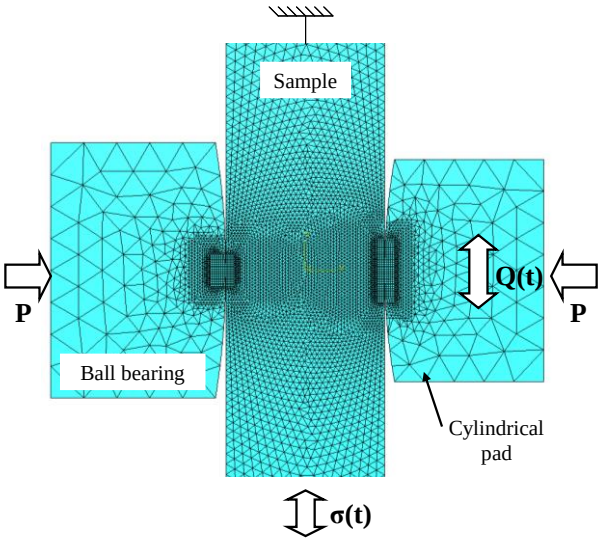

Figure 7. FEM fretting fatigue model with R2 pad; contact mesh size ℓ=100µm

Both the loading and boundary conditions were imposed to reproduce the experimental test situations. Figure 8 illustrates the loading sequences during the computation. First, a static fatigue loading is imposed. Then, the normal force is applied to the ball-bearing and to the pad. Finally, the cyclic fatigue and fretting loading are imposed simultaneously and in phase, only for one cycle. Indeed the maximum Von Mises stresses related to the crack nucleation conditions are systematically below the Yield stress. This is consistent with the fact that our analysis focuses high cycle crack nucleation conditions (10^6 cycles). An elastic assumption is therefore considered so that only the first fretting cycle is computed to extract the cyclic loading path required for investigating the fatigue cracks.

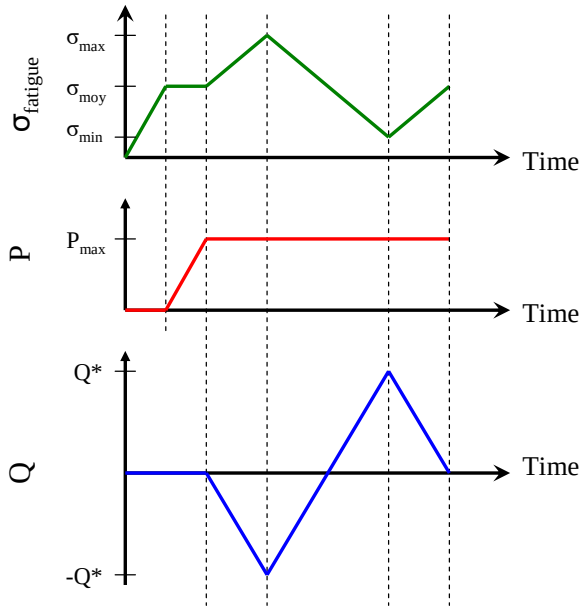

Figure 8. Loading cycle applied to the fretting fatigue model

Besides, the specimens are significantly thicker than the contact area so that each solid could be considered as an elastic half space. Hence, the Hertzian description can be applied to estimate the pressure distribution [27]. Similarly, the subsequent application of an alternating tangential force gives rise to a symmetric shear traction distribution that is similar to that described by Mindlin and Deresciewicz [28]. The contact pressure contribution is assumed to be constant and static due to very small displacement amplitude. The description of the cyclic shear contribution is more complex, defined as a superposition of different elliptic distributions to describe the pulsing evolution of the sliding front from the external contact border to the inner stick boundary. Hence, symmetrical shear stress field distributions are alternatively imposed at the tangential force amplitude +Q* and –Q* (Figure 9.a).

Under fretting fatigue condition, symmetrical shear stress field distributions are alternately imposed at tangential force amplitudes +Q* and –Q* depending on the bulk fatigue loading. By contrast to the plain fretting condition, the dissymmetry of the sliding domain due to the addition of the fatigue loading promotes a dissymmetry of the shearing profiles by introducing an offset of the sticking zone (Figure 9.b).

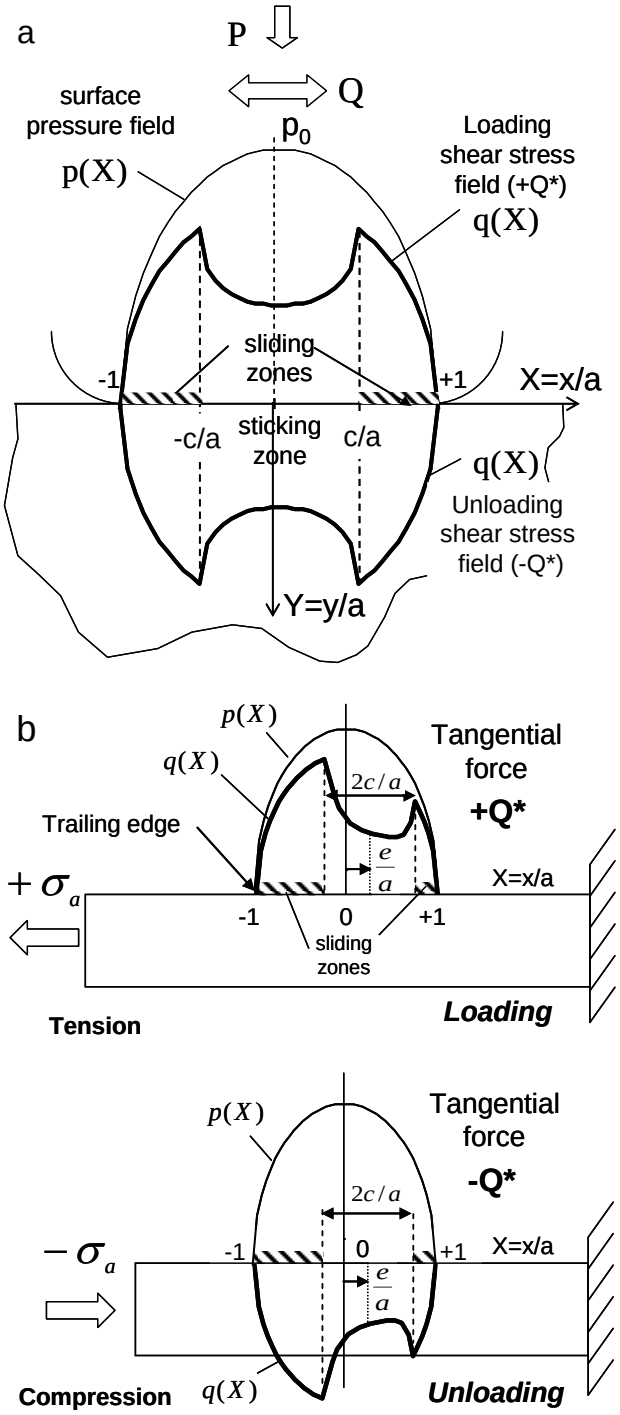

Figure 9. Illustration of pressure and shear stress field distribution: (a) plain fretting condition; (b) Fretting fatigue condition [6]

3.2. Mesh size effect

An analysis of the quadratic mesh size effect in contact areas was performed in Finite Element Modelling. The subsurface profile of the maximal principal stress ($\sigma_{1,max}$) operating at the trailing edge (x = -a) for the maximum loading state related to the crack nucleation condition

($Q^* = Q^*_{CN\_exp}$) is computed for each experimental condition (i.e. cylinder radius, and fatigue loading). Note that the symmetrical shear stress imposed by the plain fretting loading leads to similar stress profiles at each contact border:

$$\sigma_{1,\max}(x=-a,z,Q=+Q^*) = \sigma_{1,\max}(x=a,z,Q=-Q^*) \quad \textbf{(2)}$$

The introduction of bulk stressing under fretting fatigue conditions promotes a relative deformation in the fatigue specimen compared to the fretting pad which induces a shift of the sticking zone. This offset leads to a non symmetrical distribution of the surface shear stress field and consequently a non symmetrical distribution of the principal stress so that:

$$\sigma_{1,\max}(x=-a,z,Q=+Q^*) > \sigma_{1,\max}(x=a,z,Q=-Q^*) \quad \textbf{(3)}$$

The maximal stress $\sigma_{1,max}$ over a fretting cycle was computed for a chosen experimental condition (Pad R2, $p_0 = p_{ref}$ and $Q^* = Q^*_{CN\_exp}$). Figure 10 displays the depth profile of the maximal stress at the trailing edge (x = -a) for the different mesh sizes investigated from 5µm to 100µm. The results show a strong mesh size dependence on the contacting surface. The computed maximal stress, at the surface, decreases when the mesh size is increased. By contrast, the principal stress below the surface gives good correlation for all meshes used. In fact, the surface node is strongly mesh size dependent, but whatever this size, the second node in depth joins up with the finest mesh and even with the exact solution provided by the analytical formulation extracted from the Mindlin – Mc Evans expressions [7].

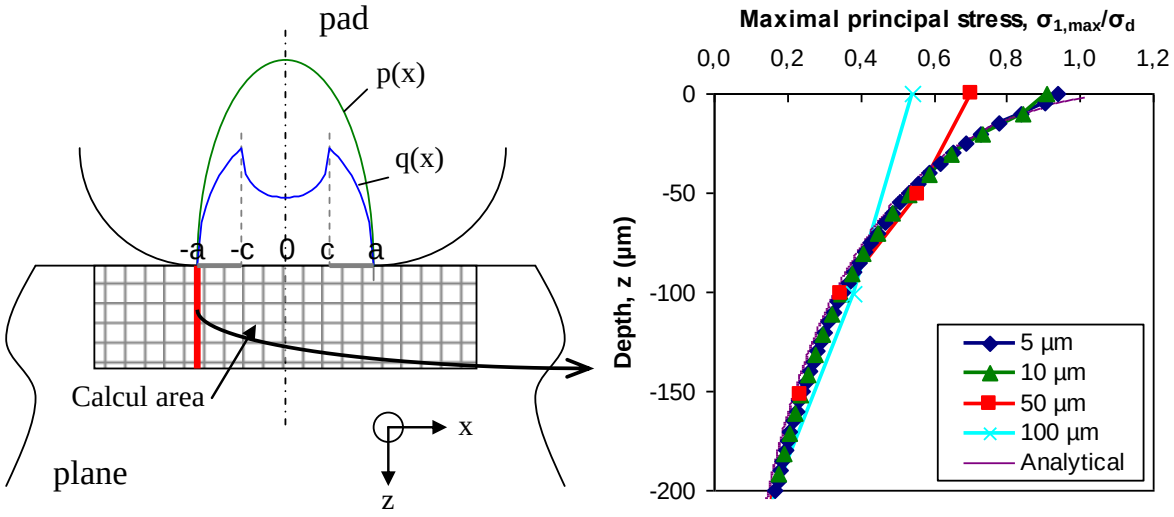

Figure 10. Mesh size effect on stress profiles (Plain fretting test, pad R2, $p_0=p_{ref}$ and $Q^*=Q^*_{CN\_exp}$)

To quantify the error induced by the mesh size on the stress field estimation, FEM profiles were compared to an analytical calculation of the same loading condition (Plain fretting loading; pad R2; p_0/p_{ref} = 1.00 and $Q^* = Q^*_{CN\_exp}$). Figure 11 gives the errors between FEM and analytical results. These errors are defined as:

$$\%\sigma_{1,\max} = \frac{\sigma_{1,\max}(z,\ell) - \sigma_{1,\max}(z,A)}{\sigma_{1,\max}(z,A)} \quad \textbf{(4)}$$

With $\sigma_{1,\max}(z,\ell)$ the maximal stress determined using the FEM model and $\sigma_{1,\max}(z,A)$ the maximal stress defined analytically. "z" is the considered depth of the computation, "ℓ" is the mesh size and "A" means "analytical method".

At the surface, the FEM results are different from the analytical ones. The larger the mesh size, the greater the difference with the exact analytical solution. At 100µm in depth, mesh size has no influence on the result, neither when one mesh size is compared to another, nor when FEM is compared to analytical results. The error is constant and less than 10%. A small gap prevails because analytical computations assume a semi infinite condition which is not the case for Finite Element analysis which considers the exact geometry of the specimens. A major conclusion of this analysis is that the FEM stress computation diverges at the surface (probably due to numerical instabilities related to contact interactions) but is converging to the exact solution at the second node in depth of the model.

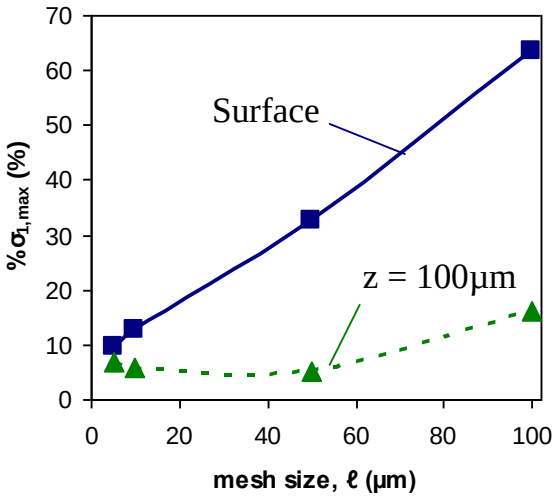

Figure 11. Errors between analytical and FEM results at the surface and at z = 100µm

3.3. Maximal stress computation

Based on this analysis and on practical aspects, it was arbitrarily decided to consider the maximal principal stress at a depth z = 100µm for the different studied mesh sizes (i.e. from 5µm up to 100µm). Note that a 5µm mesh size corresponds to about the grain size of the tested material and a 100µm mesh size is the fixed size to export the model to industrial systems and so to keep a reasonable calculation duration for very complex model geometries. The stress gradient, between the surface and the depth of 100µm, was also estimated. For the first approximation a linear evolution of the stress profile was assumed so the stress gradient was defined as the difference between the maximal stress at the surface (z = 0µm) and the maximal stress at z = 100µm divided by 100µm, the depth between these two points:

$$\nabla\sigma_{1,\max} = \frac{\sigma_{1,\max}(z = 0\mu m) - \sigma_{1,\max}(z = 100\mu m)}{100\mu m} \quad \textbf{(5)}$$

Figure 12 reports these results as a function of the mesh size from 5µm to 100µm. 5µm corresponds to about the grain size of the titanium alloy used (Point A) whereas 100µm is the imposed mesh size to be able to export models to industrial contexts (Point B). This graph shows that the maximum tensile stress remains constant at a depth of z = 100µm, whatever the mesh size. This confirms our previous conclusion that after the second node below the surface, the stress computation is not mesh size dependent. By contrast, the stress gradient decreases with the increase of mesh size. This parameter is therefore mesh size dependent. In this case, it could be possible to predict the crack nucleation threshold by applying the critical distance based on the maximal stress computation at the depth of 100µm.

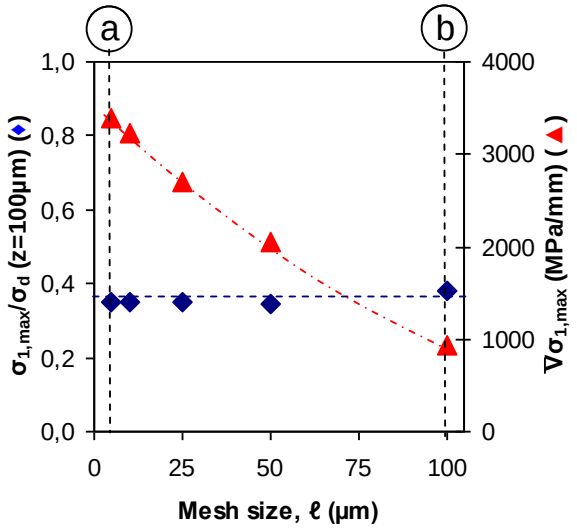

Figure 12. Maximal stress and stress gradient according to mesh size in FEM

4. Critical distance analysis

The crack nucleation risk was first calculated using the conventional critical distance analysis. To avoid stress discontinuity on the top surface, the stress state which is considered for the crack nucleation analysis is defined at ℓ_{CD} below the surface, at the trailing edge of the contact (Figure 13). In this section, the chosen depth was arbitrarily fixed at ℓ_{CD} = 100µm and the maximal stress computation was analysed to predict the cracking nucleation threshold.

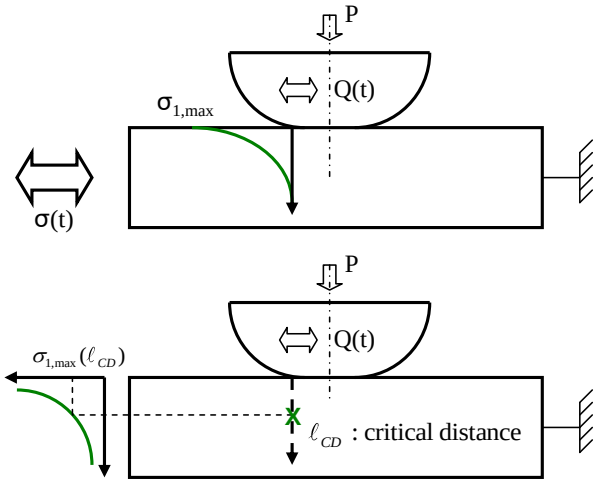

Figure 13. Illustration of the critical distance approach in fretting fatigue

The first step was to calibrate the methodology on one experimental crack threshold. The chosen reference condition is the experimental crack nucleation threshold obtained with the cylinder R2 under plain fretting loading at $p_0 = p_{ref}$. With this calibration, the critical maximal stress σ_{1,max_c} can be determined. In a given configuration, if the maximal stress computed at 100µm deep is lower than the critical maximal stress σ_{1,max_c}, there is no risk of cracking. By contrast, if the computed maximal stress is higher than the critical value, there is a risk of crack nucleation.

The critical maximal stress was determined for an experimental crack nucleation condition. Then, the critical distance analysis was used for plain fretting tests and for fretting fatigue experiments (R2 and R3). The results were compared to experimental cracking thresholds in Figure 14.a. In this graph the broken line corresponds to a perfect correlation between numerical and experimental results. Only the reference point, used to define the critical maximal stress, is aligned on it. Other crack nucleation thresholds are rather far from the correlation line. This suggests that the critical distance approach is not pertinent to take into account the stress gradient imposed below the contact. Indeed, for given loading parameters, decreasing the pad size leads to an increase of the stress gradient below the contact. The critical distance approach, which does not directly include in its formulation the stress gradient parameter, does not appear pertinent to capture the very high stress gradients induced by fretting stress. To quantify the difference between experimental and numerical results, the following error parameter is introduced:

$$Error(\%) = \frac{Q_{CD} - Q^*_{CN\_\exp}}{Q^*_{CN\_\exp}} \cdot 100 \qquad \textbf{(6)}$$

Where Q_{CD} is the predicted crack nucleation threshold and $Q^*_{CN\_exp}$ the experimental crack nucleation condition. A negative error means that the prediction is not conservative compared to experimental results whereas a positive error means a conservative prediction. Figure 14.b confirms that the critical distance methodology is not optimum to take into account the stress gradient induced by contact stress. The error factor ranges from -45% to -35% for the smaller pad and from +15% to +70% for the larger one. The errors computed for the intermediate pad size are quite small with a maximum of +30%. As mentioned previously, the crack nucleation prediction needs to take into account the stress gradient induced by the contact. However, the introduction of the stress gradient parameter induces a mesh size dependence in the model. An alternative strategy is to consider the maximal stress computed at a critical distance (ℓ_{CD} =

100µm), but also the stress gradient parameter corrected for the mesh size effect by coupling a weight function and a mesh size coefficient.

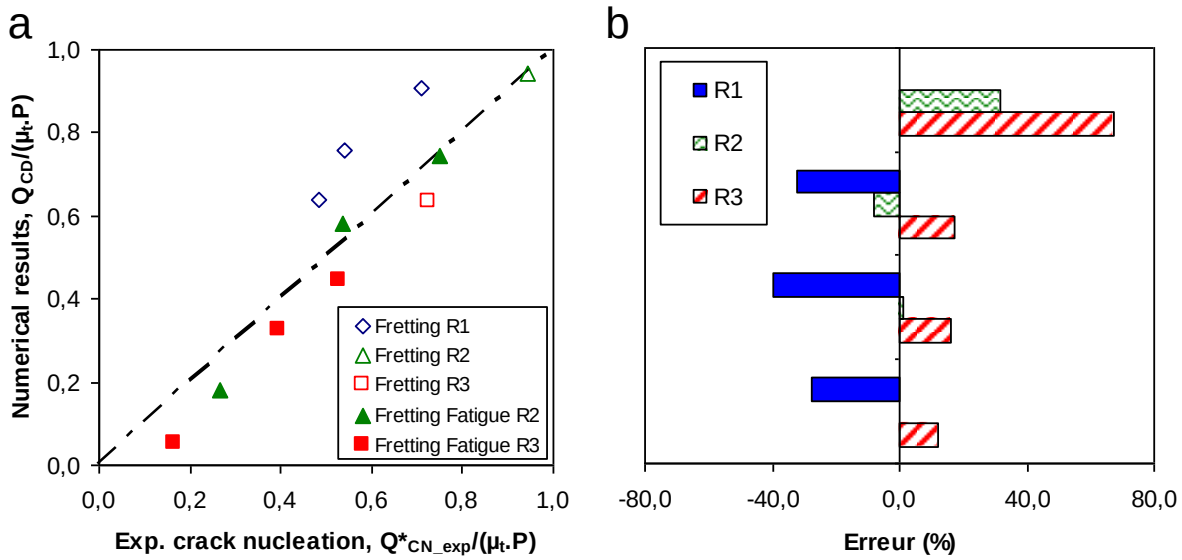

Figure 14. a: Numerical results vs. Experimental ones; b: Error between experimental and numerical results

5. Introduction of a "principal stress – weight function" approach

5.1. Proposal

The key point of our crack nucleation prediction analysis is to take into account the stress gradient effect, avoiding the mesh size effect. A proposal is thus introduced to consider these two parameters in the cracking prediction. This proposal is based on the maximal stress computed at a depth of 100µm and multiplied by a weight function which is stress gradient dependent. The cracking risk is therefore defined by:

$$\sigma_{1,\max}(z=100\mu m)\times w<\sigma_d \qquad (7)$$

with $\sigma_{1,max}$(z = 100µm), the maximal stress at 100µm in depth, σ_d the alternating bending fatigue limit and w the introduced weight function. This weight function is considered as in a linear relation with the stress gradient. Hence, the weight function can be written thus:

$$w=1+k(\ell)\cdot\nabla\sigma_{1,\max} \qquad (8)$$

Where $\nabla\sigma_{1,\max}$ is the mean stress gradient between the surface and the depth of 100µm. It has been shown that this element is mesh size dependent. In order to correct this dependency, a

coefficient $k(\ell)$, also mesh size dependent, is introduced. The proposed approach is now fully defined by:

$$\sigma_{1,\max}(z=100\mu m)\times\left(1+k(\ell)\cdot\nabla\sigma_{1,\max}\right)<\sigma_d \quad \textbf{(9)}$$

This model is rather simple since only one parameter is introduced. It takes into account the stress gradient effect in the cracking prediction and it avoids the mesh size dependence of the stress gradient through the use of the weight function. Moreover the cracking risk is defined by comparison with a material parameter, the alternating bending fatigue limit.

5.2. 5 µm mesh size analysis

The proposal was first applied to the 5µm mesh size models. The k(ℓ) parameter, defined as a correction coefficient for the mesh size effect, needs to be defined from experimental data. k(ℓ=5µm) is experimentally determined using experimental thresholds (Figure 15). The relation between the weight function and the stress gradient is assumed to be linear. In this configuration, the coefficient k(ℓ=5µm) is defined as equal to $4{,}34.10^{-4}$ $MPa^{-1}.mm$.

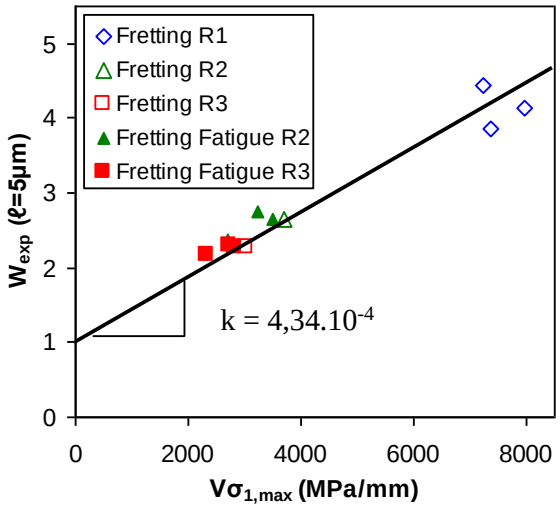

Figure 15. Weight function value according to the stress gradient (ℓ = 5µm)

Based on this coefficient value, crack nucleation thresholds were computed and compared to the experimental values. In Figure 16.a the x-axis plots the experimental crack nucleation condition and the y-axis the predicted crack initiation boundary. Very good correlation between experimental and numerical results is achieved so that all the points are aligned along

the correction line. The stress gradient imposed by the contact is taken into account well by this approach. To confirm the good prediction of the proposal, the prediction errors were computed and presented in Figure 16.b. The errors do not exceed 5% which underlines the high stability of this approach. Only two situations display a discrepancy are higher than 20% and correspond to fretting fatigue tests characterized by the highest fatigue stressing and consequently the smallest fretting loading (i.e. the smallest stress gradient).

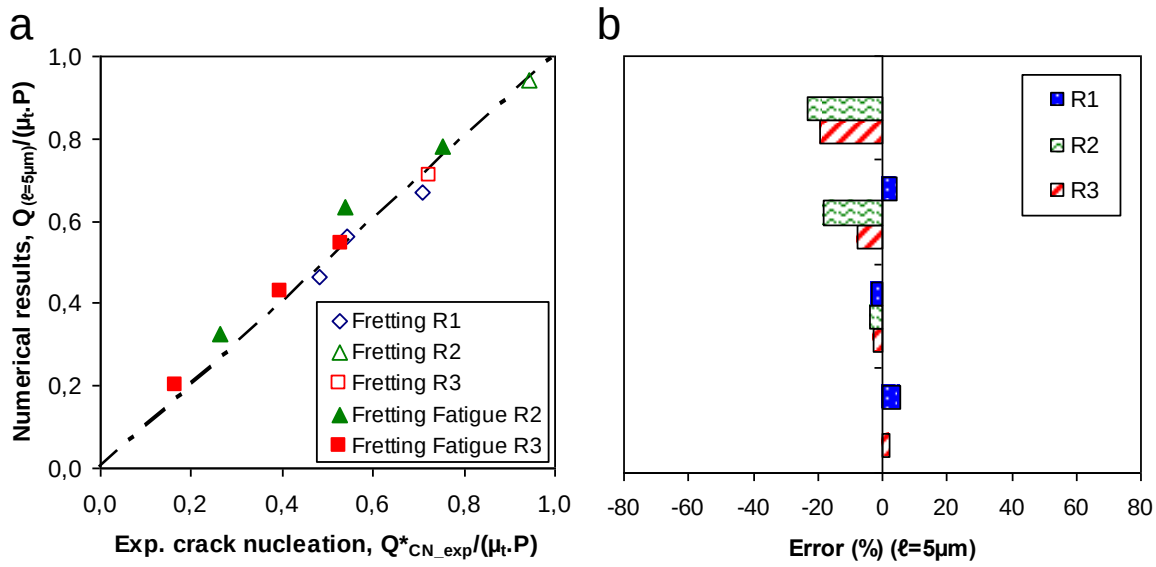

Figure 16. a: ℓ=5µm numerical results vs. experimental ones; b: Error between experimental and numerical results

5.3. 100 µm mesh size analysis

Good predictions have been obtained using very fine meshing (ℓ=5µm) representative of the microstructure. A critical aspect is to verify if such an approach can be transposed to predict the crack nucleation risk using larger mesh sizes like the ones usually applied in engineering design (ℓ=100µm). One important point of this proposal is to avoid the mesh size effect. To calculate the crack initiation conditions, the corresponding k(ℓ=100µm) coefficient first needs to be evaluated. A similar methodology to that developed for the fine meshing (ℓ=5µm) is transposed to the new meshing ℓ = 100µm. Figure 17 confirms a linear correlation between the weight function and the stress gradient. The obtained value k(ℓ=100µm) is higher than k(ℓ=5µm) because the computed stress gradients are obviously smaller for the larger mesh size. Moreover, the scattering induced by numerical computation is also higher. However the

linear correlation could easily be determined. In this configuration, k(ℓ=100µm) is defined as $2{,}07.10^{-3}$ $MPa^{-1}.mm$.

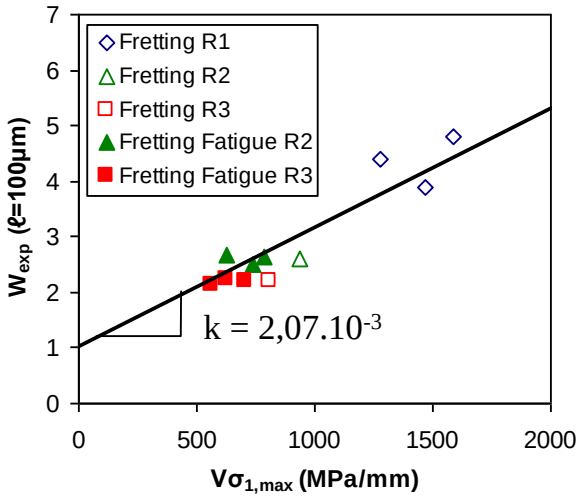

Figure 17. Weight function value as a function of the stress gradient (ℓ =100µm)

Using the new k(ℓ) parameter, the predicted crack nucleation conditions are compared to the experimental data (Figure 18.a). Once again, very good linear correlation is observed, which suggests that a precise estimation of the cracking risk can be obtained by considering a representative value of the k(ℓ) parameter, whatever the stress conditions (Fretting Fatigue and plain fretting) and the cylinder radius (i.e. stress gradient conditions). Besides, the errors do not exceed 17% which is much better than the prediction given by the plain critical distance analysis. One interesting conclusion of this work is that, thanks to the weight function correction, the reliability of the crack nucleation prediction is not affected by the mesh size interference. Indeed, very good predictions are obtained even with very coarse contact meshing.

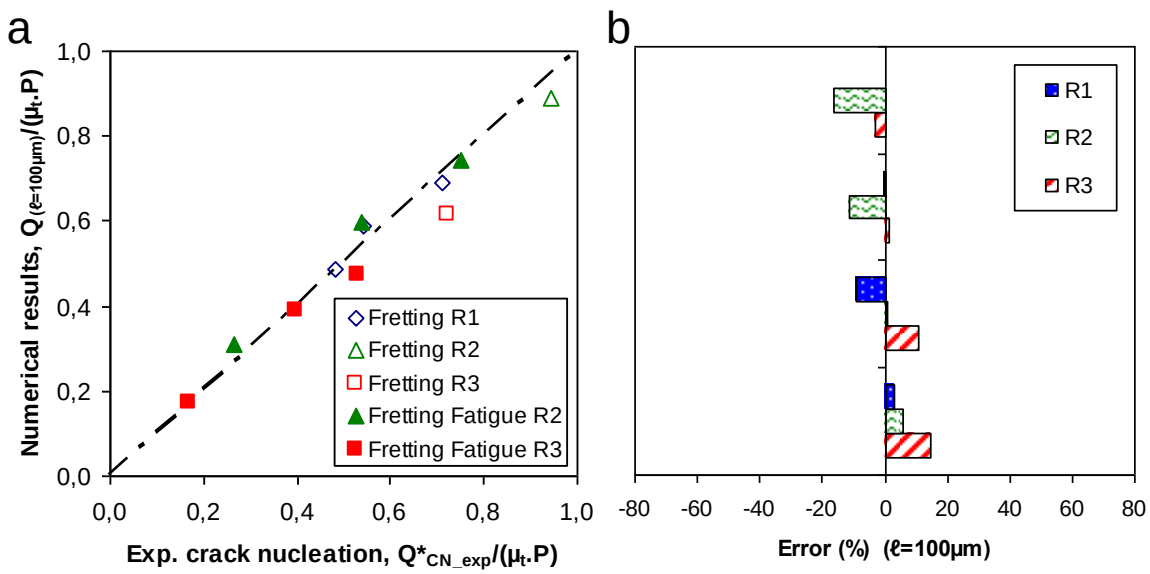

Figure 18.a: ℓ=100µm numerical results vs. experimental ones; b: Error between experimental and numerical results

6. Discussion

The aim of this paper was to propose a new approach to predict the crack nucleation risk induced by fretting fatigue stressing, using Finite Element Modelling. The use of a FEM methodology imposes the choice of a reduced mesh size of the contact area. This implies very long calculation times. The proposed criterion, which consists in combining a critical distance analysis with a weight function approach, allows us to obtain a good prediction of the crack nucleation risk whatever the mesh size. To validate the methodology, two quadratic mesh sizes were compared:

- ℓ = 5µm: this mesh size corresponds to about the grain size of the Ti-10V-2Fe-3Al titanium alloy tested in this paper. It gives a good compromise between running time and precision of the results, for simple 2-dimensional geometries.
- ℓ = 100µm: this mesh size is imposed by our industrial application. It is the minimal mesh size industrial stress departments can use to determine the cracking risk of complex components.

Our methodology shows that the criterion takes into account mesh size. Hence, using a larger mesh size allows the computation time to be drastically reduced and therefore larger industrial systems to be analyzed. Figure 19.a compares the cracking prediction obtained with a 5µm

mesh size below the contact, with the 100µm mesh size prediction. There are little differences between the two predictions (Figure 19.b). Although the maximal error, which is less than 15%, is observed for the 100µm mesh size analysis, the latter appears to be more conservative than the prediction provided by the 5µm computations. In fact all the results are aligned along the correlation line so it can be concluded that the given strategy takes into account the stress gradient effect below the contact and corrects its mesh size dependency by introducing a specific weight function.

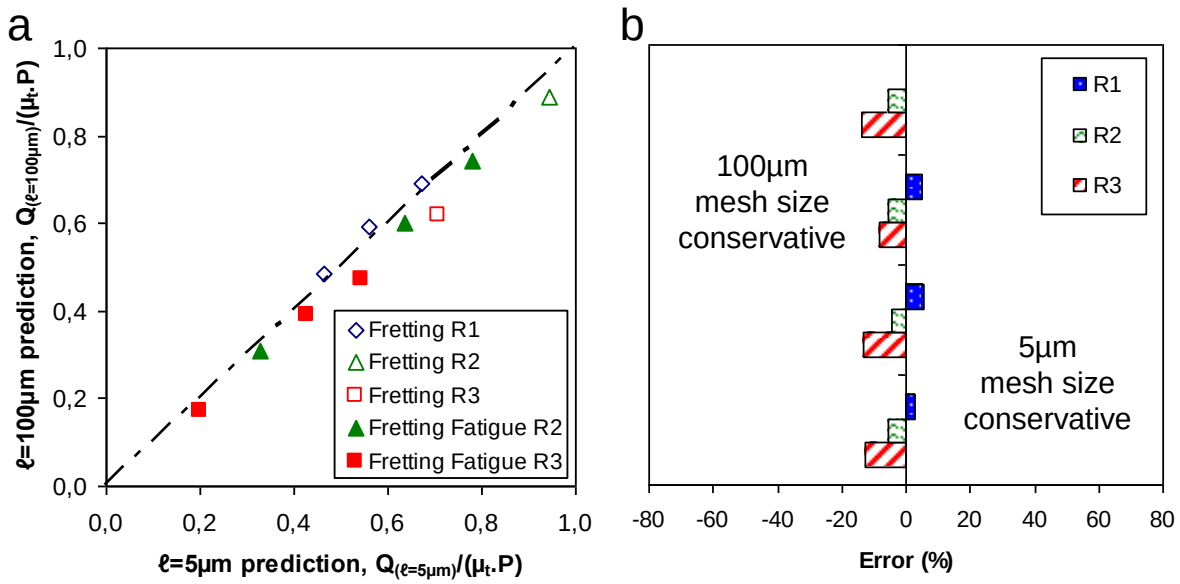

Figure 19. (a) Comparison between 5µm mesh size prediction and 100µm mesh size prediction; (b) Error between the two numerical results

7. Conclusion

In this paper, plain fretting and fretting fatigue crack nucleation thresholds were experimentally determined for a cylinder on plane configuration. Tests were performed using different radii of cylinders, changing the stress gradient below the surface. The addition of bulk fatigue loading also highlights the effect of the fatigue loading on the crack nucleation condition.

Based on these experimental results, a degraded numerical approach was proposed to predict the crack nucleation threshold of a titanium alloy for plain fretting and fretting fatigue

loadings. This original proposal is based on the maximal stress value imposed during a fretting cycle and presents numerous advantages:

- The proposal is very simple: it is based on the determination of the maximal stress at a specific depth below the surface, corrected by a weight function.
- The weight function includes stress gradient effects in plain fretting and in fretting fatigue loadings. The use of this function in the proposal gives good correlations with experimental crack nucleation thresholds, avoiding the mesh size effect in FEM Modelling.
- In Finite Element Modelling, the stress gradient value, calculated from the surface, is highly mesh size dependent. The proposed weight function includes that. The proposal provides the possibility of analysing larger industrial systems by increasing the mesh size.

New developments shall however be undertaken to better understand why such basic maximal principal stress provides so stable predictions. Besides, more elaborated strategies implying amplitude and mean stress components will be investigated to see if they can improve again the predictions. Finally multiaxial approaches like Crossland [8] or Dang Van [29] modellings will be compared in order to evaluate the potential gain in fretting cracking predictions provided by such complex formalisms compared to the given very basic uniaxial stress description.

Acknowledgement

The author wishes to thank Eurocopter France for its financial support and also thanks J. Panter, M. Taillandier and T. Van Dorsselaere for their remarks on and support of this work.

References

[1] R. B. Waterhouse, “Fretting debris and elamination theory of wear,” *Wear,* vol. 29, pp. 337-344, 1974.

[2] S. Fouvry, “An energy description of wear mechanisms and its applications to oscillating sliding contacts,” *Wear,* vol. 255, no. 1-6, pp. 287-298, Sep. 2003.

[3] S. Fouvry, P. Dùo, and P. Perruchaut, “A quantitative approach of Ti?6Al?4V fretting damage: friction, wear and crack nucleation,” *Wear*, vol. 257, no. 9-10, pp. 916-929, Nov. 2004.

[4] O. Vingsbo and S. Söderberg, “On fretting map,” *Wear*, vol. 126, pp. 131-147, 1988.

[5] S. Fouvry, P. Kapsa, and L. Vincent, “Quantification of fretting damage,” *Wear*, vol. 200, pp. 186-205, 1996.

[6] S. Fouvry and K. Kubiak, “Introduction of a fretting-fatigue mapping concept: Development of a dual crack nucleation – crack propagation approach to formalize fretting-fatigue damage,” *International Journal of Fatigue*, vol. 31, no. 2, pp. 250-262, Feb. 2009.

[7] D. A. Hills and D. Nowell, “Mechanics of fretting fatigue,” *Kluwer Academic Publishers*, 1994.

[8] B. Crossland, “Effect of large hydrostatic pressure on the torsional fatigue strength of an alloy steel,” *in proc. of int. conf. on fatigue of metals, London*, 1959.

[9] K. N. Smith, P. Watson, and T. H. Topper, “A stress-strain function for the fatigue of metals,” *Journal of Materials*, vol. 5, pp. 767-778, 1970.

[10] C. Navarro, S. Munoz, and J. Dominguez, “On the use of multiaxial fatigue criteria for fretting fatigue life assessment,” *International Journal of Fatigue*, vol. 30, no. 1, pp. 32-44, Jan. 2008.

[11] H. Neuber, “Therory of notch stresses: principles for exact calculation of strength with reference to structural form and material,” *2nd ed Berlin: Springer Verlag*, 1958.

[12] R. E. Peterson, “Notch sensitivity,” *In. Sines G, Waisman JL, editors. Metal fatigue. New York: Mc Graw Hill*, pp. 293-306, 1959.

[13] L. Susmel, “The theory of critical distances: a review of its applications in fatigue☆,” *Engineering Fracture Mechanics*, vol. 75, no. 7, pp. 1706-1724, May. 2008.

[14] D. Taylor, “The theory of critical distances☆,” *Engineering Fracture Mechanics*, vol. 75, no. 7, pp. 1696-1705, May. 2008.

[15] S. Fouvry, P. Kapsa, F. Sidoroff, and L. Vincent, “Identification of the caracteristic length scale for fatigue cracking in fretting contact,” *Journal of Physique IV*, vol. 8, pp. 159-166, 1998.

[16] S. Fouvry, P. Kapsa, and L. Vincent, “A multiaxial fatigue analysis of fretting contact taking into account the size effect,” *Fretting Fatigue: current technology an practices, ASTM STP 1367*, pp. 167-183, 2000.

[17] H. Proudhon, S. Fouvry, and G. Yantio, “Determination and prediction of the fretting crack initiation: introduction of the (P, Q, N) representation and definition of a variable

process volume," *International Journal of Fatigue*, vol. 28, no. 7, pp. 707-713, Jul. 2006.

[18] J. Araujo, L. Susmel, D. Taylor, J. Ferro, and E. Mamiya, "On the use of the Theory of Critical Distances and the Modified Wöhler Curve Method to estimate fretting fatigue strength of cylindrical contacts," *International Journal of Fatigue*, vol. 29, no. 1, pp. 95-107, Jan. 2007.

[19] R. Amargier, S. Fouvry, L. Chambon, C. Schwob, and C. Poupon, "Stress gradient effect on crack initiation in fretting using a multiaxial fatigue framework," *International Journal of Fatigue*, vol. 32, no. 12, pp. 1904-1912, Dec. 2010.

[20] J. Araújo and D. Nowell, "The effect of rapidly varying contact stress fields on fretting fatigue," *International Journal of Fatigue*, vol. 24, no. 7, pp. 763-775, Jul. 2002.

[21] C. Lykins, "Combined experimental–numerical investigation of fretting fatigue crack initiation," *International Journal of Fatigue*, vol. 23, no. 8, pp. 703-711, Sep. 2001.

[22] K. Kubiak, S. Fouvry, and A. Marechal, "A practical methodology to select fretting palliatives: Application to shot peening, hard chromium and WC-Co coatings," *Wear*, vol. 259, no. 1-6, pp. 367-376, Jul. 2005.

[23] L. J. Fellows, D. Nowell, and D. A. Hills, "On the initiation of fretting fatigue cracks," *Wear*, vol. 205, pp. 120-129, 1997.

[24] H. Lee and S. Mall, "Investigation into effects and interaction of various fretting fatigue variables under slip-controlled mode," *Tribology International*, vol. 39, 2006.

[25] J. Meriaux, S. Fouvry, K. J. Kubiak, and S. Deyber, "Characterization of crack nucleation in TA6V under fretting–fatigue loading using the potential drop technique," *International Journal of Fatigue*, vol. 32, no. 10, pp. 1658-1668, Oct. 2010.

[26] D. Nowell and D. A. Hills, "Mechanics of fretting fatigue tests," *Int Jnl Mech Sci*, vol. 29, no. 5, pp. 355-365, 1987.

[27] K. L. Johnson, "Contact mechanics," *Cambridge University Press*, 1985.

[28] R. D. Mindlin and H. Deresciewiecz, "Elastic sphere in contact under varying oblique forces," *International Journal of Fatigue*, vol. 27, no. 5, pp. 569-579, 2005.

[29] K. Dang Van, "Macro-micro approach in high-cycle multiaxial fatigue," *Advances in Multiaxial Fatigue, ASTM STP 1191*, pp. 120-130, 1993.